Effects of Protein Aggregation in Isocratic Nonlinear Chromatography

Roger D. Whitley, Kevin E. Van Cott, James A. Berninger, and N.-H. Linda Wang
School of Chemical Engineering, Purdue University, West Lafayette, IN 47907

A versatile reaction-separation (VERSE) model was developed to quantitatively simulate the behavior of chromatographic separations coupled with reactions. Detailed mass transfer and reaction mechanisms are considered. Aggregation data of myoglobin and β-lactoglobulin A verified the model. The effects of concentration, equilibrium distribution, reaction rate, convection rate, particle radius, and relative affinity are shown for a dimerizing system. When the aggregation rate is relatively slow compared with convection and mass transfer rates, the individual forms behave as separate species in frontal, elution, and displacement chromatography. For rapid aggregation rates, the individual forms behave as a single component with an average affinity. The wave asymmetry and increased spreading due to aggregation depend on relative affinity differences. Serious error may result if aggregation is overlooked in parameter estimation using frontal or pulse analysis. The dimensionless group principles developed here are useful in scaling and predicting when peak or wave splitting or merging will occur in reaction chromatography systems.

Introduction

General characteristics of aggregation in separations

An exciting challenge in using chromatography for protein purification is to understand the interplay of solution-phase reactions and separation dynamics. For traditional small ion separation, reactions do not occur in the separation step, unless specifically promoted. Proteins and other macromolecules, however, often undergo aggregation or conformational changes during chromatography—usually against the desires of the chromatographer. The aggregates formed almost always exhibit different chromatographic behavior from their constituents, resulting in additional or oddly shaped peaks. Keller and Giddings (1960) noted that many of these aggregate forms were misinterpreted as impurities in some of the first chromatograms of large biological compounds. In that work, they also presented some simple modeling of how the peak shape of two interconverting forms would appear under fast and slow conversion rates; however, mass transfer effects were not considered. Reaction of an enantiomer with a chiral selector has been intentionally induced in the area of chiral separations with great success (Krull, 1978; Lindner et al., 1979; Weinstein et al., 1982)—more to the delight of the chromatographer.

The characteristics of aggregation pose challenges on two scales. Analytically, peaks assumed pure may broaden or split, rendering peak identification difficult. Industrially, scaling is complicated by the flow rate and concentration dependences of aggregation. Researchers have conducted a number of experimental studies of aggregating protein systems in chromatography (Kunitani et al., 1988; Karger and Blanco, 1989; Grinberg et al., 1989; Blanco et al., 1989). Special challenges are posed in pH gradient operation since the gradient makes use of the protonation-deprotonation reaction to change solute affinity and capacity. Some research has been reported on pH dependence: Sophianopoulos and Van Holde (1964) conducted a detailed study of pH-dependent dimerization for hen's egg-white lysozyme. The impact of pH gradients on a particular system can be studied by experimentally determining a relationship of the rate constants to pH for the system of interest, as was done in Sophianopoulos and Van Holde (1964).

Aggregation effects are not limited to chromatography. Multiple peaks and merging of peaks due to aggregation have also been observed in electrophoresis of biological molecules (Cann, 1987). There is widespread interest in the effects of aggregation in polymer and surfactant systems (Menger, 1979; Chakrabarti

Correspondence concerning this article should be addressed to N.-H. L. Wang.

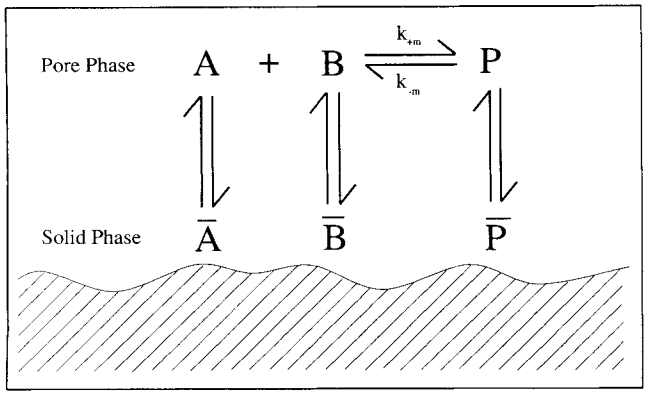

Figure 1. Heteroaggregation in chromatography.

and Toral, 1989). Some traditional techniques for studying aggregation behavior are sedimentation and low-angle laser light scattering (LALLS) (Bruzzesi et al., 1965; Stuting et al., 1989; Mhatre et al., 1990). Kihara and Tsuruta (1988) have characterized both aggregation kinetics and conformational changes by stopped flow X-ray scattering. Garcia-Rubio (1989) has conducted a detailed study on the use of spectroscopic techniques to characterize protein aggregation. We have classified the products of an aggregation reaction as either homoaggregates or heteroaggregates. Both of these types present special challenges in separations.

Heteroaggregation

Heteroaggregation, which is the aggregation of two or more different solutes (see Figure 1), is quite common in protein systems. Chromatographing tumor necrosis factor (TNF) in the presence of its partially proteolyzed (14-kD) fragment results in the appearance of two more peaks. Kunitani et al. (1988) have shown that the peaks, in the order they elute, are: 1. the TNF trimer; 2. a heterotrimer of TNF and the 14-kD fragment in a 2:1 ratio; 3. the TNF monomer; and 4. the 14-kD fragment. The second peak is an example of heteroaggregation. Experimental study of hemoglobin tetramers dissociating reversibly into $\alpha\beta$ dimers has been conducted by Baudin-Chich et al. (1988). This phenomenon can greatly reduce the resolution of solutes which form heteroaggregates.

As mentioned earlier, chiral compounds have been introduced into mobile-phase solutions to selectively complex with chiral solutes. Primary applications of this induced aggregation have been in the separation of amino acids into their chiral forms (Lindner et al. 1979; Weinstein et al., 1982) and of pharmaceuticals in general (Pettersson et al., 1987; Davankov, 1989).

Homoaggregation

Homoaggregation is the formation of aggregates from one solute (Figure 1, with *A* and *B* identical). Elution of these aggregates may give either broad or multiple peaks. Many proteins exhibit homoaggregation; some examples are lysozyme (Bruzzesi et al., 1965; Imoto et al., 1972), β-lactoglobulin A (β-lact A) (Blanco et al., 1989), concanavalin A (Olson and Liener, 1967; McKenzie et al., 1972), human serum albumin (Anspach et al., 1990), and TNF (Kunitani et al., 1988). One of the systems that will be studied in this work is the hydrophobic interaction chromatography (HIC) of β-lact A. The extent of aggregation has been studied as a function of pH, concentration and temperature (Blanco et al., 1989).

High concentration effects

As protein concentration increases, specific aggregation reactions give way to random clustering of molecules. This clustering may progress until precipitation occurs. The effect has been observed through studies of standard-state free energy changes for serum albumin, ovalbumin, and aldolase (Muramatsu and Minton, 1989). The resulting chromatographic peaks are broad due to the wide distribution of binding forms. Insulin exhibits such nonspecific aggregation for a variety of experimental conditions, both with metal coions such as zinc (Coffman and Dunn, 1988) and without such ions (Jeffrey et al., 1976). Because of the importance of insulin in animal metabolism, its chemical and structural properties have been extensively studied (Blundell et al., 1972; Chothia et al., 1983). Some chromatographic study of insulin has also been reported (Gross et al., 1988; Kroeff et al., 1989; McLeod et al., 1990), but little has been done to characterize the effect of metal coions on chromatographic behavior. This type of nonspecific aggregation will not be considered further in the current study and is mentioned here for its completeness.

Current status of reaction-separation modeling

Much experimental work has been done on the aggregation of proteins. Even though aggregation can have a profound effect on protein separation, little in the way of combined quantitative aggregation-separation modeling has been presented. Langer et al. (1969) comprehensively reviewed applications of reactions in gas chromatography, with its focus on reaction kinetics using chromatographic reactors. No band spreading due to mass transfer effects was considered in the model, and the analysis is limited to linear isotherm systems. Karger et al. (1980) reviewed aggregation, as well as many other types of what they call "secondary chemical equilibria," in chromatography. Since the principal focus of the articles reviewed was on the reactions, the underlying mass transfer effects were not detailed and in most cases reaction rates were assumed to be much faster than mass transfer rates. The study by Keller and Giddings (1960) assumed a linear isotherm model and probability distribution between two possible forms. Klinkenberg (1961) explained band broadening in terms of slow, reversible reactions for the first-order reaction kinetics and rapid mass transfer.

Several more recent studies on reaction separation systems have taken advantage of the simplicity of multicomponent local equilibrium theory. Golden et al. (1974) studied selectivity reversal due to complexation in a three-component system. Klein (1981) simulated neutralization and precipitation reactions of small ions. In the same NATO Proceedings, Villermaux (1981) studied general reaction kinetics in chromatography. More recently, Hwang et al. (1988) presented a detailed mathematical development for general combined separation-reaction processes. Unfortunately, multicomponent equilibrium theory does not consider mass transfer effects, which are usually important for large molecules (Kirkby et al., 1986; Whitley et al., 1989b).

Loureiro et al. (1983) presented a study of solid-phase re-

actions in fixed beds and observed shifts in solute retention due to irreversible reaction. Endo and Wada (1983) used a stage model to consider both solution and solid-phase reactions for zone-interference chromatography. A series of papers, focused on size-exclusion chromatography, applied simple stage models to study kinetic effects on peak splitting (Zimmerman, 1974; Stevens, 1986; Stevens, 1989). Cann (1987) proposed a set of simultaneous mass transport and reaction equations to model the hybridization and dimerization of proteins in zone electrophoresis. That study included the case of fast conversion between the two forms, allowing for dynamic equilibrium. In all these cases, the mass transfer limitations of chromatography were either assumed negligible or approximated by numerical dispersion.

Hsu and Ernst (1990) have presented a fast Fourier transform (FFT)-based column model, which considers the effects of axial dispersion but is limited to linear isotherms and first-order solution phase reactions. Those limits are commonly violated for biochemical separations and aggregating systems. Furthermore, the model makes no allowance for a concentration profile within the particle. In addition to the effects of slow intraparticle diffusion (which are common for high molecular weight molecules), reactions in both the solution phase and solid phase may also cause large concentration gradients to develop inside the porous particles. Goto et al. (1990) question whether a parabolic concentration profile alone is sufficient when reactions are present. Their findings indicate that for reactants diffusing into the particle (such as in chromatography), parabolic profiles are accurate only for Biot numbers and Thiele moduli less than unity.

Scope of current research

For the current study, we employ the general rate model with a multicomponent Langmuir isotherm. Axial dispersion, film mass transfer, and intraparticle diffusion are considered. Coupled continuity and reaction equations were solved numerically using orthogonal collocation on finite elements. Reacting systems of two or three components are studied under isocratic operating conditions. The effects of aggregation on all three operating modes of chromatography (frontal, elution, and displacement) are investigated. The frontal mode consists of a step up in concentration into an initially unloaded column, which is often used for the estimation of isotherm parameters and the removal of impurities. Elution chromatography involves the application and subsequent elution of a pulse of solute(s), which is widely used for the analysis of complex mixtures and the separation of biochemicals from complex media. Displacement chromatography uses a displacer to force off and concentrate a pulse of solute(s) which has been applied to a column (Cramer and Horváth, 1988). Homoaggregation (dimerization) and heteroaggregation reactions are examined. The general rate model, modified to include both solution and solid-phase reactions, is called the versatile reaction-separation (VERSE) Model. Because the scope of reaction separations is broad, the current study focuses on solution-phase reactions in chromatography.

Key Results

The proposed model was verified by comparing with two other experimental systems (myoglobin breakthrough and β-lact A elution). Using dimerization as a model system, we methodically elucidated the interplay between aggregation and chromatographic separation. The dependence of peak splitting on the flow rate, retention time, equilibrium distribution, and concentration is similar for all single-reaction homoaggregating systems. The dimensionless group approach was used to interpret the results. When the ratio of reaction rate to the controlling mass transfer rate is greater than unity, peaks tend to merge. Heteroaggregation serves as an example where reactions may be driven in the thermodynamically unfavored direction through application of Le Châtelier's principle. Since heteroaggregation requires two or more reactants, peak resolution depends strongly on relative retention times. Subsequently, we explained how aggregation may hamper or facilitate a separation process.

VERSE Model

General rate model

The VERSE model represents an integrated approach to reaction-separation modeling. The details of numerical simulation, including convergence of the solutions, have been presented elsewhere (Whitley, 1990). Rate model equations that consider axial dispersion, film mass transfer, and intraparticle diffusion are used to describe the chromatography process. The fundamental rate modeling of nonreacting chromatography systems has been presented by Yu and Wang (1989) and Lee et al. (1989). Modules were added to allow for generation or consumption of each species (each aggregation state of a solute is treated as a unique component in the model) based on a user-selected set of kinetic expressions. The resulting equations are Eqs. 1 and 2.

Bulk Phase

$$\frac{\partial c_{b_i}}{\partial \theta} = \frac{1}{Pe_b}\frac{\partial^2 c_{b_i}}{\partial x^2} - \frac{\partial c_{b_i}}{\partial x} + \upsilon_{b_i} - N_{f_i}\,(c_{b_i} - c_{p_i,\xi=1}) \tag{1a}$$

$$x=0,\ \frac{\partial c_{b_i}}{\partial x} = Pe_b\,(c_{b_i} - c_{f_i}) \tag{1b}$$

$$x=1,\ \frac{\partial c_{b_i}}{\partial x} = 0 \tag{1c}$$

$$\theta=0,\ c_{b_i} = c_{b_i}(0, x) \tag{1d}$$

Pore Phase

$$Ke_i\left[\epsilon_p\frac{\partial c_{p_i}}{\partial \theta} - \epsilon_p\,\upsilon_{p_i}\right] + (1+\epsilon_p)\left[\frac{\overline{C}_{T_i}}{C_{e_i}}\right]\upsilon_{l_i} = N_{p_i}\frac{1}{\xi^2}\frac{\partial}{\partial \xi}\left[\xi^2\frac{\partial c_{p_i}}{\partial \xi}\right] \tag{2a}$$

$$\xi=0,\quad \frac{\partial c_{p_i}}{\partial \xi} = 0 \tag{2b}$$

$$\xi=1,\quad \frac{\partial c_{p_i}}{\partial \xi} = Bi_i\,(c_{b_i} - c_{p_i}) \tag{2c}$$

$$\theta=0,\quad c_{p_i} = c_{p_i}(0,\xi) \tag{2d}$$

Throughout the column, plug flow and constant temperature are assumed; viscous fingering and surface diffusion are not accounted for by this model. The terms v_{b_i} and v_{p_i} represent a generation of species i by aggregation in the mobile and pore phases, respectively. Dimensionless numbers will be defined and discussed once all of them have been presented. The v_{ℓ_i} term is isotherm-dependent. If the solid-phase concentrations are in equilibrium with the solution-phase concentrations which are directly adjacent (no slow adsorption or desorption), then Eq. 3 applies, and an equilibrium isotherm may be used to obtain v_{ℓ_i}.

$$v_{\ell_i} = \sum_{j=1}^{N_c} \left[\frac{\partial \bar{c}_{p_i}}{\partial c_{p_j}} \frac{\partial c_{p_j}}{\partial \theta} \right] \tag{3}$$

The mobile-, pore- and solid-phase concentrations are scaled as follows:

$$c_{b_i} \equiv \frac{C_{b_i}}{C_{e_i}}; \quad c_{p_i} \equiv \frac{C_{p_i}}{C_{e_i}}; \quad \bar{c}_{p_i} \equiv \frac{\bar{C}_{p_i}}{\bar{C}_{T_i}}$$

where C_{e_i} is the maximum possible entering concentration for specie i (if the equilibrium distribution of all reactions were shifted to favor production of i completely) and $\bar{C}_{T_i}$ is the maximum solute capacity for specie i. C_{P_i} is the pulse concentration. Dimensionless column length, x, is defined as $x \equiv z/L$, and dimensionless particle distance, ξ, is defined as $\xi \equiv r/R$. Dimensionless time is $\theta \equiv t/\tau$, where τ is the time required for one bed volume of solution to pass through the column (percolation time) (Eq. 4).

$$\tau \equiv \frac{L}{u_o} \tag{4}$$

Reaction equations

An aggregating system is more complex than a multicomponent system without reaction due to the interconversion between the various states of aggregation. Each aggregate of a particular protein is treated as an individual component in the isotherm. One form of a solute can compete with another form; the sorbent may also have a different capacity and affinity for each form. Reaction kinetics may vary widely among protein systems. Fortunately, the kinetic expressions are similar, regardless of the particular solute under consideration.

To allow for a wide variety of aggregation reactions, the VERSE model uses a set of basic reactions (Eq. 5), from which more complex sequences may be built.

$$A \rightleftharpoons P \tag{5a}$$

$$2A \rightleftharpoons P \tag{5b}$$

$$3A \rightleftharpoons P \tag{5c}$$

$$A + B \rightleftharpoons P \tag{5d}$$

$$A + 2B \rightleftharpoons P \tag{5e}$$

For general study, we consider the case of a protein which interconverts between monomer and dimer forms, denoted as M and D (Eq. 6), which is, of course, based on Eq. 5b.

$$2M \underset{k_{-m}}{\overset{k_{+m}}{\rightleftharpoons}} D \tag{6}$$

The corresponding concentrations for M and D are C_{b_M} and C_{b_D} with an appropriate kinetic expression (Eq. 7).

$$v_{b_M} = -2 \left[N_{k_{+m,M}} c_{b_M}{}^2 - N_{k_{-m,M}} c_{b_D} \right] \tag{7a}$$

$$v_{b_D} = \left[N_{k_{+m,D}} c_{b_M}{}^2 - N_{k_{-m,D}} c_{b_D} \right] \tag{7b}$$

For the dimer reaction, $C_{e_M} = 2C_{e_D}$, since total conversion of the dimer from monomer would require two moles of monomer for one mole of dimer. The resulting dimensionless reaction rates can be seen in Table 1. The equilibrium distribution is defined by:

$$K_m = \frac{k_{+m}}{k_{-m}} = \frac{C_{b_D}}{C_{b_M}^2} \tag{8}$$

where k_{+m} and k_{-m} are the forward and reverse reaction constants, which are based on one unit of dimer produced (Eq. 6). The reaction expressions are written for the mobile phase; each corresponding pore-phase expression is obtained by substituting v_{p_i} for v_{b_i} and C_{p_i} for C_{b_i}. Breakup of the protein aggregates can be caused by shear stresses under high flow rates. This effect is not explicitly accounted for in the current implementation of VERSE. One could add an additional consumption term in the mobile-phase equation to account for shear-induced breakup if this effect is important.

Multicomponent Langmuir isotherm

Careful selection of isotherms to represent the often complex behavior of aggregating systems is crucial. The multicomponent Langmuir isotherm describes a range of experimental data well (Blanco et al., 1989):

$$\bar{C}_{p_i} = \frac{a_i C_{p_i}}{1 + \sum_{j=1}^{N_c} b_j C_{p_j}} \tag{9}$$

This is a simple isotherm form that allows both affinity and maximum sorbent capacity to be uniquely set for each solute. In general, each aggregate form will have an affinity and sorbent capacity different from the other forms. The dimerizing system studied in this work has this characteristic. For the cases in which another isotherm is known to describe a system more accurately, the model can be readily adapted to a wide range of isotherms.

Selection of mass transfer parameter values

Because of the detailed mass transfer aspects considered by this rate model, there are three mass transfer parameters which must be determined (E_b, k_{f_i}, and E_{p_i}). E_b is calculated from Pe_b, where Pe_b is estimated from the correlation (Chung and Wen, 1968):

$$Pe_b = \frac{L}{2\epsilon_b R} (0.2 + 0.011 Re^{0.48}) \tag{10}$$

Table 1. Relative Rates Characterized by Dimensionless Groups*

Numerator/Divisor	Convection	Film Mass Transfer	Intraparticle Diffusion
Axial Dispersion	$\frac{1}{Pe_b}=\frac{E_b}{u_oL}$		
Film Mass Transfer	$N_{f_i}=3\left(\frac{L}{R}\right)\frac{(1-\epsilon_b)k_{f_i}}{\epsilon_b u_o}$	1	$Bi_i=\frac{k_{f_i}R}{E_{p_i}}$
Intraparticle Diffusion**	$N_{pi}=\left(\frac{L}{R}\right)\left(\frac{1}{Pe_{p_i}}\right)$		1
Forward Reaction (Monomer Basis)	$N_{k_{+m,M}}=\frac{Lk_{+m}C_{e_M}}{u_o}$	$Da_{k_{+m,M}}=\frac{Rk_{+m}C_{e_M}}{k_{f_M}}$	$\Phi^2_{k_{+m,M}}=\frac{R^2k_{+m}C_{e_M}}{E_{p_M}}$
Reverse Reaction (Monomer Basis)	$N_{k_{-m,M}}=\frac{1}{2}\cdot\frac{Lk_{-m}}{u_o}$	$Da_{k_{-m,M}}=\frac{1}{2}\cdot\frac{Rk_{-m}}{k_{f_M}}$	$\Phi^2_{k_{-m,M}}=\frac{1}{2}\cdot\frac{R^2k_{-m}}{E_{p_M}}$
Forward Reaction (Dimer Basis)	$N_{k_{+m,D}}=4\cdot\frac{Lk_{+m}C_{e_D}}{u_o}$	$Da_{k_{+m,D}}=4\cdot\frac{Rk_{+m}C_{e_D}}{k_{f_D}}$	$\Phi^2_{k_{+m,D}}=4\cdot\frac{R^2k_{+m}C_{e_D}}{E_{p_D}}$
Reverse Reaction (Dimer Basis)	$N_{k_{-m,D}}=\frac{Lk_{-m}}{u_o}$	$Da_{k_{-m,D}}=4\cdot\frac{Rk_{-m}}{k_{f_D}}$	$\Phi^2_{k_{-m,D}}=\frac{R^2k_{-m}}{E_{p_D}}$

*Reaction expressions are for a dimerization reaction.

**$Pe_{p_i}=\frac{u_oR}{E_{p_i}}$

and the Reynolds number, Re, is defined as:

$$Re=\frac{2R\rho u_o\epsilon_b}{\mu} \tag{11}$$

The film mass transfer coefficient, k_{f_i}, depends on Re; in the systems being studied, Re is typically less than 0.1. Thus, the correlation developed for low Re values by Wilson and Geankoplis (1966) is appropriate for k_{f_i} estimation (Eq. 12).

$$J=\left(\frac{k_{f_i}}{u_o\epsilon_b}\right)Sc_i^{2/3}=\frac{1.09}{\epsilon_b}Re^{-2/3} \tag{12}$$

The Schmidt number is defined as:

$$Sc_i=\frac{\mu}{\rho D_i^\infty} \tag{13}$$

E_{p_i} may be estimated from Brownian diffusivity, D_i^∞, by Eq. 14 (Mackie and Meares, 1955; Helfferich, 1983).

$$E_{p_i}=\left(\frac{\epsilon_p}{2-\epsilon_p}\right)^2 D_i^\infty \tag{14}$$

Equation 14 was developed from a study of small ions, however, and does not always hold well for protein molecules. Often, E_{p_i} is treated as an adjustable parameter for experimental data. Tyn and Gusek (1990) offer a comprehensive source of the D_i^∞ values for proteins.

Solution of the VERSE model

The differential equations of the VERSE model are discretized by the application of orthogonal collocation on fixed finite elements. The axial direction (Eq. 1) is divided into 50–60 elements, each with four interior collocation points; Legendre polynomials are used for each element. For the radial direction into the particle (Eq. 2), only one element is required and it is described by a Jacobi polynomial with two interior collocation points. Simulations of these systems with three interior collocation points showed no change from two point simulations. The resulting set of ordinary differential equations, associated algebraic boundary conditions, and reaction equations are solved by a differential/algebraic system solver (DASSL) (Petzold, 1982). This solution scheme has proved to be robust in dealing with complex sets of stiff, coupled equations; more details of the solution and convergence checks may be found in Whitley (1990).

Characteristic dimensionless groups

The key to understanding aggregation (or any other reaction) in flow systems such as chromatography lies in understanding relative rates. Whether or not a reaction is "fast" depends on the time available for the reaction; the time availability in turn depends on the convection rate and the mass transfer rate. Lee et al. (1989) have conducted an in-depth study of key dimensionless groups for mass transfer in isocratic elution systems without aggregation. Those groups, plus additional dimensionless groups arising from solution-phase reactions, are written as the ratios of rates and serve as a guide to which the rate phenomenon dominates the behavior of a given system (see Table 1). The Thiele modulus, Φ_k^2, represents a ratio of reaction rate to intraparticle diffusion rate; it is equivalent to N_k/N_p. The N_{p_i} and N_{f_i} groups are interdependent (Lee et al., 1989).

Results and Discussion

To focus on the effects of aggregation, most of the systems chosen for simulation have relatively fast film mass transfer and intraparticle diffusion rates. The amount of band spreading due to axial dispersion is small and does not significantly

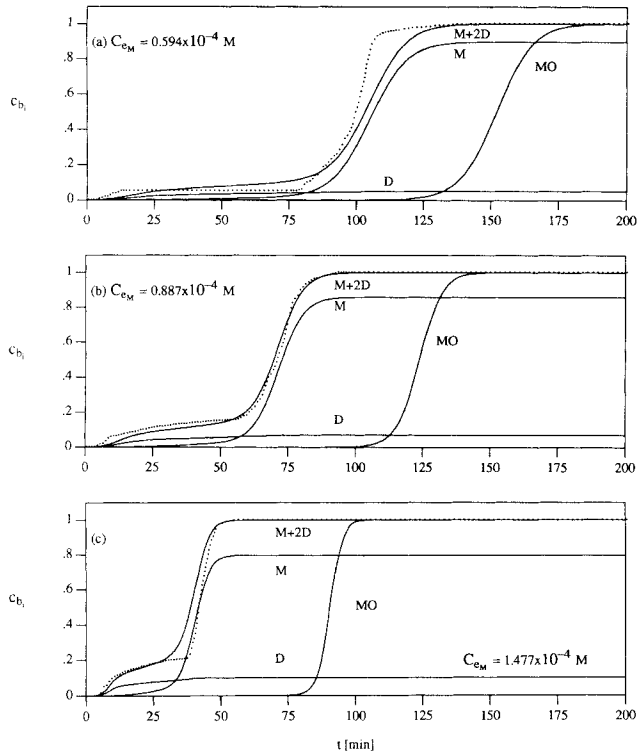

Figure 2. Experimental breakthrough of myoglobin on an immobilized metal affinity (IMAC) column (. . . .) and model simulation as a dimerizing system (——).

alter peak resolution for the current study. For clarity, the systems addressed in this work show specific interactions as opposed to nonspecific clustering. The reactions for specific interactions are few and readily derived from kinetic and mass balance studies.

Homoaggregation

Mass Balance and Verification. The mass balance for the simulations showed a maximum error of 0.05%; this is within the error tolerances set for the various routines used in the computations. Next, the case of no reaction was compared to that of dimerization. The equilibrium constant for the dimerization was set to favor either monomer or dimer in the extreme. In both cases, the resulting chromatogram becomes identical to that of one component without reaction. In addition, model simulations are compared with the data from two different chromatography systems in the following sections.

Study of Myoglobin. The first experimental system studied was a series of breakthrough curves of myoglobin on an immobilized metal affinity chromatography (IMAC) column. Details of the experiments can be found elsewhere (Wong, 1990). The experimental curves are shown in Figure 2. The distinctive feature of these experiments is the two-plateau breakthrough curve, resulting from the injection of what appears to be a monomer-dimer mixture at equilibrium. This shape suggests two components, but as concentration changes, the relative heights of these two plateaus change, suggesting an aggregation reaction.

As a first approximation to this system, it was assumed that a simple dimerization was occurring, and the extinction coefficient was assumed twice as great for the dimer as for the monomer. The resulting simulations are also shown in Figure 2, and the associated experimental and simulation parameters are shown in Table 2. The simulations closely approach the response of the experimental system to concentration changes, including the rounded nature of the leading front. The possibility exists that there could be a small amount of higher-order aggregates in the system, but a monomer-dimer system explains the major characteristics of the chromatogram. Similar behavior was observed for a breakthrough curve of human serum albumin by Anspach et al. (1990). The effects of such breakthrough curves on parameter estimation will be discussed in a later section.

The diffuse part of the first wave and the slow approach to saturation could be due to slow adsorption and desorption effects. This explanation is supported by the small value of E_p required to fit the data. Agreement with the data may be improved by considering slow adsorption and desorption effects, which are beyond the scope of this article and have been discussed elsewhere (Wong, 1990).

Since all aggregation reactions involve the combination of at least two molecules, the dimensionless reaction rates also depend on concentration, which is clearly shown in the definitions of $N_{k_{+m}}$ and $Da_{k_{+m}}$ (Table 1). As shown by a simulation in Figure 2, increasing the inlet concentration causes an earlier average breakthrough of the front, just as for a single component. The leading front of the breakthrough curve, however, does not elute much earlier and merges with the larger, second front. Even though there are two forms of the solute, the breakthrough curve begins to take on the appearance of a single-component systems, since higher concentration gives a higher effective reaction rate. Comparing to a case of no dimerization (same system parameters, without the dimerization reaction), the MO (monomer only) curve has a much more delayed breakthrough time and less change in breakthrough time with concentration than the dimerizing system. Implication of the dimerization reaction on parameter estimation will be discussed later.

Study of β-lactoglobulin A. Under the experimental conditions reported in Karger and Blanco (1989), injection of pure β-lact A results in three peaks which are, in the order they elute, a dodecamer, a tetramer, and an octamer. In the sim-

Table 2. Parameters for Myoglobin-IMAC Simulation

Reaction		
Eq. 6	$k_{+m}=4.0\ M^{-1}\cdot s^{-1}$	$k_{-m}=3.73\times10^{-3}s^{-1}$
Langmuir Isotherm		
Parameter	Monomer	Dimer
a	85.0	10.0
b [M^{-1}]	$1.5\times10^{+4}$	$3.0\times10^{+5}$
System		
L [cm]	7.5	
R [cm]	5.0×10^{-4}	
u_o [$cm\cdot s^{-1}$]	0.0993	
ϵ_b	0.38	
ϵ_p	0.81	
D_i^∞ [$cm^2\cdot s^{-1}$]	1.1×10^{-6}	5.5×10^{-7}
E_{p_i} [$cm^2\cdot s^{-1}$]	5.0×10^{-9}	5.0×10^{-10}

Table 3. Dimensionless Groups for β-lact A Reactions (Eq. 17)*

Y	$N_{k_{+m}}$	$N_{k_{-m}}$	$N_{k_{+n}}$	$N_{k_{-n}}$
Y_4	$\frac{Lk_{+m}C_{e_4}}{u_o}$	$\frac{1}{2}\cdot\frac{Lk_{-m}}{u_o}$	$\frac{1}{2}\cdot\frac{Lk_{+n}C_{e_4}}{u_o}$	$\frac{1}{3}\cdot\frac{Lk_{-n}}{u_o}$
Y_8	$4\cdot\frac{Lk_{+m}C_{e_8}}{u_o}$	$\frac{Lk_{-m}}{u_o}$	$2\cdot\frac{Lk_{+n}C_{e_8}}{u_o}$	$\frac{2}{3}\cdot\frac{Lk_{-n}}{u_o}$
Y_{12}			$\frac{9}{2}\cdot\frac{Lk_{+n}C_{e_{12}}}{u_o}$	$\frac{Lk_{-n}}{u_o}$

*$Da_k=\frac{Ru_o}{k_{f_i}L}\cdot N_k$

ulations, the following stoichiometric equations developed by Grinberg et al. (1989) will be used:

$$2P_4 \underset{k_{-m}}{\overset{k_{+m}}{\rightleftharpoons}} P_8, \quad K_m=(2.4\pm0.5)\times10^4\ \mathrm{M}^{-1} \tag{15a}$$

$$P_4+P_8 \underset{k_{-n}}{\overset{k_{+n}}{\rightleftharpoons}} P_{12}, \quad K_n=(3.3\pm0.8)\times10^3\ \mathrm{M}^{-1} \tag{15b}$$

This pair of equations have both sequential and parallel characteristics; the corresponding sets of generation terms are first shown with dimensions (Eq. 16) so that the origin of the stoichiometrically-dependent dimensionless groups may be seen.

$$\left[\frac{\partial C_4}{\partial t}\right]_{RXN}=-2(k_{+m}C_4^2-k_{-m}C_8)-(k_{+n}C_4C_8-k_{-n}C_{12}) \tag{16a}$$

$$\left[\frac{\partial C_8}{\partial t}\right]_{RXN}=(k_{+m}C_4^2-k_{-m}C_8)-(k_{+n}C_4C_8-k_{-n}C_{12}) \tag{16b}$$

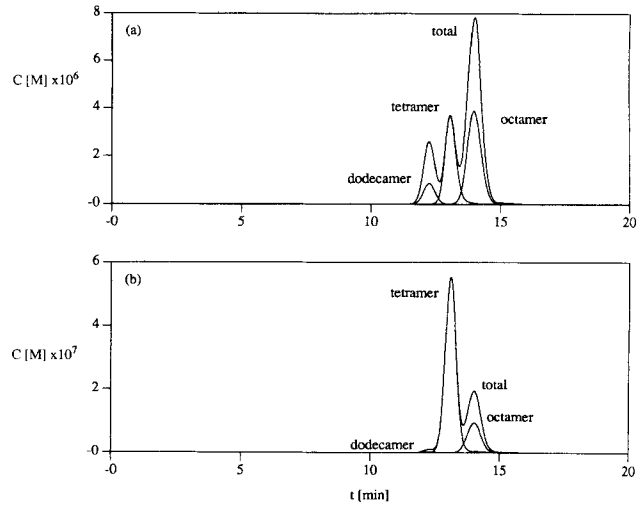

Figure 3. Simulation results of a β-lact A system based on Karger and Blanco (1989); C [M] = 2.717×10^{-4} (a) and 1.359×10^{-5} (b).

$$\left[\frac{\partial C_{12}}{\partial t}\right]_{RXN}=(k_{+n}C_4C_8-k_{-n}C_{12}) \tag{16c}$$

On conversion to dimensionless form, these equations may be written as:

$$Y_{b_4}=-2(N_{k_{+m,4}}c_{b_4}^2-N_{k_{-m,4}}c_{b_8})-(N_{k_{+n,4}}c_{b_4}c_{b_8}-N_{k_{-n,4}}c_{b_{12}}) \tag{17a}$$

$$Y_{b_8}=(N_{k_{+m,8}}c_{b_4}^2-N_{k_{-m,8}}c_{b_8})-(N_{k_{+n,8}}c_{b_4}c_{b_8}-N_{k_{-n,8}}c_{b_{12}}) \tag{17b}$$

$$Y_{b_{12}}=N_{k_{+n,12}}c_{b_4}c_{b_8}-N_{k_{-n,12}}c_{b_{12}} \tag{17c}$$

where $N_{k\pm m}$ and $N_{k\pm n}$ are dimensionless reaction rates, defined in Table 3.

Table 4. Parameters for β-lact A Simulation*

Reactions				
Eq. 15a Eq. 15b	$k_{+m}=4.0\ \mathrm{M}^{-1}\cdot\mathrm{s}^{-1}$ $k_{+n}=0.55\ \mathrm{M}^{-1}\cdot\mathrm{s}^{-1}$		$k_{-m}=1.67\times10^{-4}\mathrm{s}^{-1}$ $k_{-n}=1.67\times10^{-4}\mathrm{s}^{-1}$	
Langmuir Isotherm				
Parameter	P_4	P_8	P_{12}	
a	7.1	7.65	6.6	
b [M^{-1}]	500.0	320.0	500.0	
System				
L [cm]	10.0			
R [cm]	2.5×10^{-4}			
V_P [mL]	0.02			
u_0 [$\mathrm{cm}\cdot\mathrm{s}^{-1}$]	0.264			
ϵ_b	0.38			
ϵ_p	0.65			
D_i^∞[$\mathrm{cm}^2\cdot\mathrm{s}^{-1}$]	3.59×10^{-5}	7.19×10^{-6}	7.19×10^{-6}	
E_{p_i} [$\mathrm{cm}^2\cdot\mathrm{s}^{-1}$]	8.33×10^{-6}	1.67×10^{-6}	1.67×10^{-6}	
C_{e_4} [M]	$N_{k_{+m,4}}$	$N_{k_{-m,4}}$	$N_{k_{+n,4}}$	$N_{k_{-n,4}}$
2.717×10^{-4}	4.117×10^{-2}	3.163×10^{-3}	2.830×10^{-3}	2.109×10^{-3}
1.359×10^{-5}	2.059×10^{-3}	3.163×10^{-3}	1.416×10^{-4}	2.109×10^{-3}

*$C_{e_4}=2C_{e_8}=3C_{e_{12}}$

The specific chromatogram under study is Figure 3c of Karger and Blanco (1989). The original experiment was conducted under gradient conditions on a hydrophobic interaction column. The simulations presented in Figure 3 match the original system conditions, conducted under isocratic conditions (see Table 4); a 2.5×10^{-4} cm particle radius was used to compensate for the broader peaks of an isocratic elution. Since the retention time for the data and the simulation is identical, the time for reaction is identical. Thus, the reaction rate constants obtained by VERSE should be valid for the literature data as well as the isocratic simulation. The distribution coefficients shown in Eq. 15 were reported by Grinberg et al. (1989) based on the assumption that the extinction coefficient is twice as large for the octamer as for the tetramer and three times as high for the dodecamer as for the tetramer. This gives weighting factors to the actual concentrations of tetramer, octamer, and dodecamer of 1, 2, and 3, respectively (the curves labeled "total" in Figure 3).

Figure 3a closely matches the relative peak ratios and retention times reported in Figure 3c of Karger and Blanco (1989), showing that the reaction kinetics of the model agree with experimentally derived values. Additionally, Figure 3b of Karger and Blanco (1989) shows the same experiment at a lower concentration; the concentration effect on reaction is mirrored by Figure 3b of this study. At a higher concentration (Figure 3a), the formation of octomer and dodecamer is favored and their corresponding peaks are more pronounced. This behavior is well predicted by VERSE. Moreover, this system contains both sequential and parallel reactions—a challenge handled well by VERSE.

Dimerization and General Study. The area of protein aggregation offers a rich assortment of behavior for study. All aggregating systems share some common traits, such as the ratio of reaction rate vs. flow rate, competition among the forms for sorbent sites, and the possibility of different retention times of the forms. These traits may be demonstrated more clearly by using the most simple example of aggregation: dimerization. The general simulation parameters for all subsequent simulations are shown in Table 5; exceptions are noted with the relevant simulations. The key dimensionless groups for studying dimerization are $Da_{k_{\pm m}}$, the Damkohler number; $\Phi^2_{k_{\pm m}}$, the Thiele modulus; $N_{k_{\pm m}}$, the ratio of reaction rate to convection rate; and N_{p_i}, the ratio of intraparticle diffusion rate to convection rate. Through the analysis of relative values of these groups, it is possible to find conditions that optimize either peak merging or peak splitting.

The equilibrium distribution between interconverting forms can change with pH or temperature. The resulting effluent history for a mixture of interconverting forms may be altered radically by this shift. In Figure 4, there is a 180-fold change in the equilibrium constant for a dimerization reaction (with $N_{k_{+m}}$ held constant at 5.50 so that the effect of equilibrium shift on reaction rate could be observed). As a result, the clearly multiform breakthrough curve for $K_m = 50{,}000\ \mathrm{M}^{-1}$ (Figure 4a, $N_{k_{-m}} = 0.0550$) takes the shape of an almost normal single-component breakthrough curve for $K_m = 275\ \mathrm{M}^{-1}$ (Figure 4c), $N_{k_{-m}} = 10.0$). A striking feature of the series is that the breakthrough time of the dimer is decreased as a result of a smaller value of K_m. As K_m approaches zero, this would in fact become a single-component (monomer) system. An analogous result would be obtained as K_m approaches infinity, with the single component then being the dimer form. As noted by $N_{k_{-m}}$ in Figure 4, the decrease in K_m is represented by an increase in k_{-m}, as opposed to a decrease in k_{+m}. Similar trends may be observed by decreasing k_{+m} with k_{-m} held constant, as long as the reaction rates remain relatively high compared to mass transfer rates.

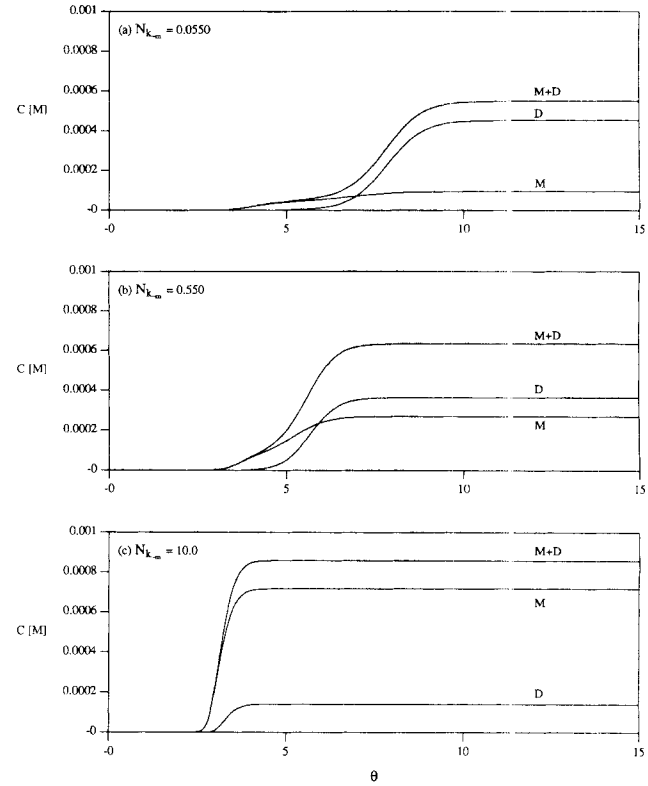

Figure 4. Effect of equilibrium shift on reaction and monomer-dimer distribution ($N_{k_{+m}} = 5.5$).

The front becomes smoother as equilibrium shifts to favor primarily monomer.

The simulated system was designed so that the convection rate is slower than the film mass transfer or intraparticle diffusion rates. In this way, the similar effects of the reaction rate and the convection rate on plateau and peak shape may be seen more clearly. Thus, the ability to resolve two or more interconverting forms depends primarily on the relative rates of reaction vs. convection ($N_{k_{\pm m}}$). Karger et al. (1980) discuss this relationship in terms of various solution-phase reactions on a qualitative basis. In this work, the effects of varying these relative rates in all three operating modes of chromatography

Table 5. General Simulation Parameters

Langmuir Isotherm			
Parameter	Monomer	Dimer	P
a	1.0	4.0	2.0
b [M^{-1}]	3,000.0	1,000.0	2,000.0
System			
L [cm]	4.0	u_o [$\mathrm{cm \cdot s^{-1}}$]	0.06063
R [cm]	2.5×10^{-3}	V_P [mL]	0.5
ϵ_b	0.35	E_{p_i} [$\mathrm{cm^2 \cdot s^{-1}}$]	2.093×10^{-7}
ϵ_p	0.60	D_i^{∞} [$\mathrm{cm^2 \cdot s^{-1}}$]	1.140×10^{-6}
C_{e_M} [M]	0.0011	$C_{e_{A,B}}$ [M]	0.0010

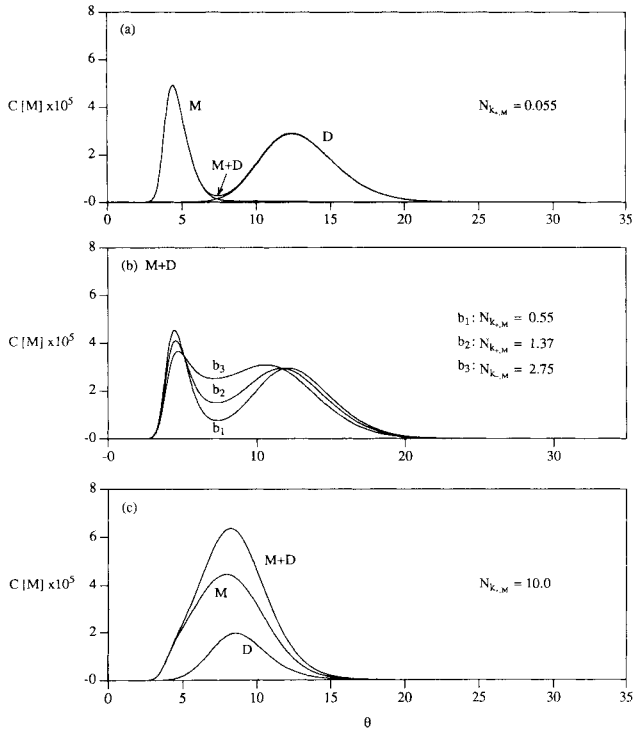

Figure 5. Reaction rate effect on peak splitting in elution mode.

As the reaction rate decreases (bottom to top), the monomer and dimer forms split to form two separate peaks.

are quantitatively shown. Moreover, the effects are easily understood and predicted through the use of dimensionless groups. In Figures 5 and 6, the interconversion rates for a dimerizing system are varied (K_m = 10^4 M^{-1}); changes in the corresponding dimensionless groups are also shown in the figures.

As the reaction rates increase (top to bottom), the two peaks of Figure 5 merge, going from two well-resolved peaks to one broad peak. Also note that the elution position of the combined

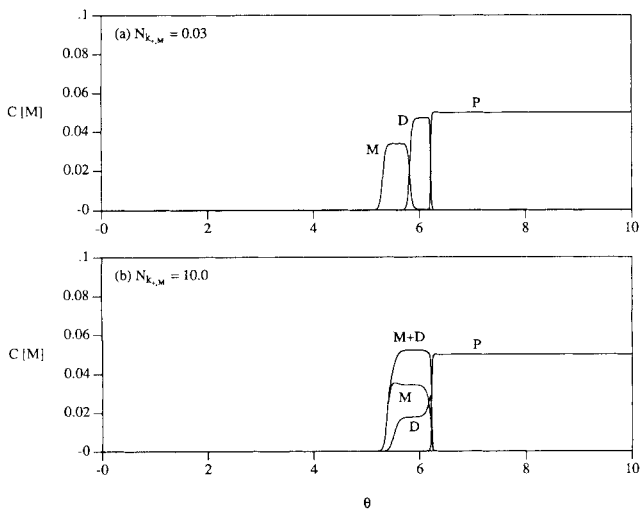

Figure 6. Displacement train for a dimerizing system.

As the reaction rate increases, the monomer and dimer bands merge into one band.

Table 6. Parameters for Dimerization Simulations Reaction Rate Series (Displacement Mode)

Langmuir Isotherm			
Parameter	Monomer	Dimer	Displacer
a	2.6	6.5	260.0
b [M^{-1}]	300.0	85.0	4,000.0
System			
L [cm]	8.0	C_{e_M} [M]	0.24
R [cm]	2.5×10^{-3}	V_P [mL]	0.5
ϵ_b	0.35	E_{p_i} [cm$^2\cdot$s^{-1}]	1.667×10^{-6}
ϵ_p	0.70	D_i^{∞}[cm$^2\cdot$s^{-1}]	5.0×10^{-5}
u_o [cm$\cdot$s^{-1}]	0.06063	K_m [M^{-1}]	15.0

peak is intermediate to well-resolved peaks. As the reaction rates become greater than the mass transfer rates, interconversion occurs at a relatively faster pace and the peaks begin to merge. The column does not "see" the monomer and dimer as two separate forms, but as a pseudosolute with an average affinity. While such a behavior has been reported in the literature, the question of "how high the reaction rates have to be for averaging to occur" has not been answered.

Looking at the dimensionless groups, one can find the answer to this question. Of the three major mass transfer rates, convection is the slowest (N_{f_i}, N_{p_i} > 1). At the slowest reaction rates (Figure 5a), $N_{k_{+m,M}}$, $Da_{k_{+m,M}}$, and $\Phi^2_{k+m,M}$ are all less than unity. As the reaction rates increase, $N_{k_{+m,M}}$ and $\Phi^2_{k+m,M}$ approach and surpass unity; $Da_{k_{+m,M}}$ also increases, but does not surpass unity because the film mass transfer rate is so high (and is thus not the controlling rate). When the reaction rates are ten times greater than the controlling mass transfer rate (convection in this case), the averaging of fronts and peaks is substantial.

Figure 6 shows the displacement mode for two different sets of reaction rates (K_m = 15.0 M^{-1}); the associated simulation parameters are shown in Table 6. The increase in reaction rates are marked by increases in $N_{k_{\pm m}}$, $Da_{k_{\pm m}}$, and $\Phi^2_{k\pm m}$. Comparing Figure 6b to 6a, one finds that the monomer and dimer peaks elute at the same time because of the higher interconversion rates. As a result, the displacement train cannot be developed. As with frontal and elution modes, the increase in this averaging effect is denoted by $N_{k_{+m}}$ and Φ^2_{k+m} as they approach and exceed unity.

Very similar changes in peak shape may also be produced by yet another phenomenon. Increasing the flow rate limits the residence time in a column, and thus limits the time for a particular reaction to occur. The result is similar to slow reaction kinetics, as may be seen by comparing Figure 7 to Figure 5 (curve b_1, the same in both figures, serves as a reference). Noting the parameters for the simulations of Figure 7, one sees that *decreasing the convection rate has a similar effect on $N_{k_{+m}}$ as increasing the reaction rates and vice versa.* Splitting of the top curve of Figure 7 is not as clean as that of Figure 5, primarily because $\Phi^2_{k+m,M}$ has increased from 0.024 to 0.24. In addition, the extra band spreading is due to mass transfer effects and is accompanied by a decrease in N_{p_i} and N_{f_i}.

As the reaction rates increase or the flow rate decreases, $N_{k_{\pm m}}$ and $Da_{k_{\pm m}}$ increase, and the two peaks merge to one broad, average peak. The peak shapes are slightly different between the two series due to intraparticle diffusion; for the flow rate series $\Phi^2_{k_{\pm m}}$ remains constant, whereas $\Phi^2_{k_{\pm m}}$ increases for the

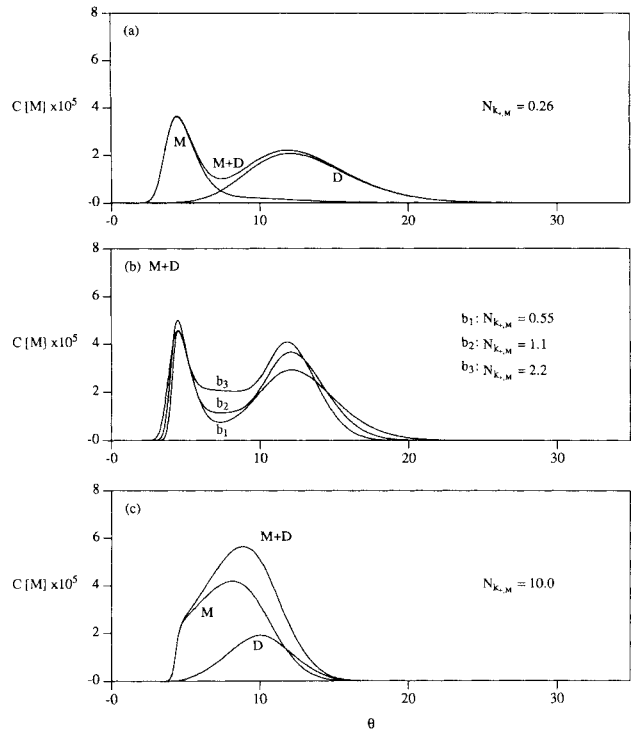

Figure 7. Convection rate effect on peak splitting.

Flow rate increases from bottom to top.

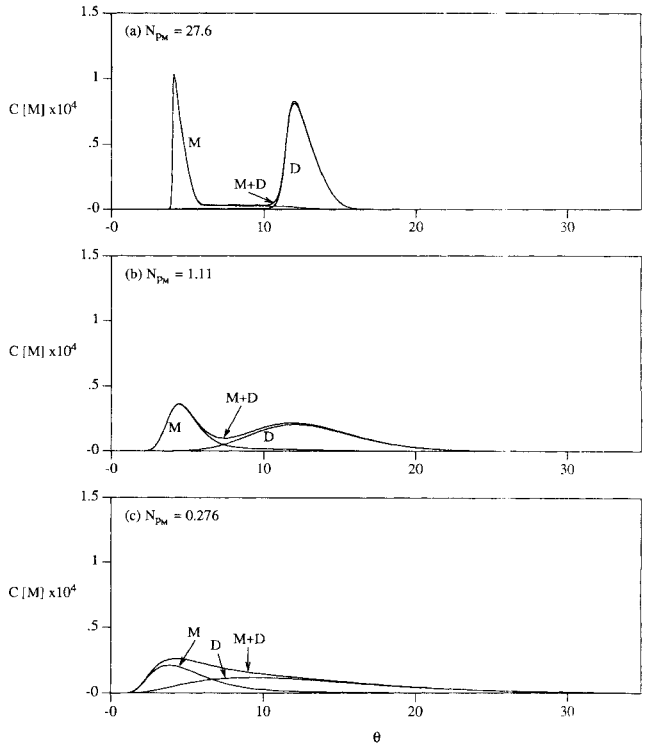

Figure 8. Intraparticle diffusion resistance effect on peak splitting through increase in particle radius.

R [cm] $= 5\times10^{-4}$ (a); 2.5×10^{-3} (b); and 5.0×10^{-3} (c).

reaction rate series. These results show the importance of the ratios of reaction rates and different mass transfer rates to the separation and resolution of the two forms.

Sorbents with small radii are used commonly to improve resolution. As can be seen in Figure 8 ($K_m = 10^4$ M^{-1}, $N_{k+m,M} = 0.2747$), *small particles also improve the resolution of aggregate forms.* The key dimensionless group to gauge this resolution is Φ^2_{k+m}, which approaches unity as R is increased from 5.0×10^{-4} to 5.0×10^{-3} cm. The intraparticle diffusion rate seems slower since there is more distance to diffuse, while the reaction rate remains constant. This change in relative rates correlates to a loss of resolution going from Figure 8a to 8c. In preparative chromatography systems, these particles sizes are larger than those of Figure 8(c). Aggregation will be less noticeable for such systems under similar operating conditions. The loss of resolution gives an apparently simple chromatograph, which can mask aggregation. The aggregation will still be able to affect retention times as a function of other system parameters, as well as degrade the accuracy of parameter estimates.

Figure 9 shows *the effect of increasing the relative affinity difference between the two forms.* The Langmuir constant a for the dimer has been increased from 4.0 to 8.0, going from Figure 5c to Figure 9; all other conditions are identical. It is interesting to note that the amount of overlap in both of the figures is roughly the same, regardless of the affinity differences of the interconverting solutes. Figure 9 demonstrates that proposed dimensionless group rules have little effect on the relative affinities of the solutes in homoaggregation systems. When the aggregation rate is relatively rapid, however, the apparent band spreading will be greater if the two forms have a large difference in affinity for the sorbent.

Effect of aggregation on parameter estimation

As has been shown by many groups, protein shape, size, and charge character strongly affect retention behavior (Fausnaugh-Pollitt et al., 1988; Blanco et al., 1989; Whitley et al., 1989a). In most cases, aggregation alters the apparent values of these physical properties. Many researchers have used the frontal analysis (of breakthrough curves) to estimate equilibrium isotherm parameters (Huber and Gerritse, 1971; Jacobson et al., 1984). If reactions, such as aggregation, occur in these systems, the accuracy of frontal analysis may be greatly compromised. Figure 2 shows that the dimerization reaction significantly changes the breakthrough time of the monomer front. Moreover, Figure 4 shows a dimerizing system for a series of equilibrium distribution values. Large change in the breakthrough time for the major vertical portion of the breakthrough

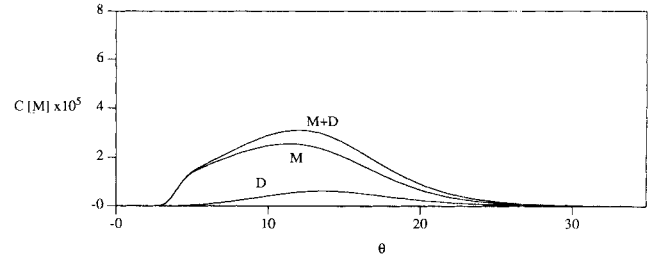

Figure 9. Effect of affinity difference on peak merging.

Difference in affinity between the two forms is increased from that of Figure 5c.

curve may be clearly seen. Any change in variables, such as concentration, temperature or pH, could cause this shift; the resulting difference in binding parameter estimates could be enormous. The flow series analog of Figure 5 would have an equally significant change in breakthrough. The apparent parameter values therefore depend on the flow rate, concentration, and particle size. Serious error in parameter estimates would again result if the aggregation effects are not considered.

Heteroaggregation

In some cases, one type of solute may aggregate with another type of solute, instead of itself (Blanco et al., 1989). This heteroaggregation can render the chromatographic separation difficult or impossible. One experimental case of this is found in the TNF system (Kunitani et al., 1988). For that system, two TNF monomer units and one 14-kD fragment combine to form a heterotrimer. The formation of the TNF heteroaggregate is also coupled with the decomposition of the trimer to a monomer. To illustrate how elution order can affect peak resolution, a simple case of heteroaggregation (Eq. 5d) was selected. A series of increasing reaction rates are shown in Figure 10 ($K_m = 2.0 \times 10^3$ M^{-1}).

In the top chromatogram, the reaction is slow and the initial equilibrium distribution is maintained. As the reaction rate increases, the system in Figure 10 behaves the opposite of a dimerizing system, where the peaks of a dimerizing system would merge into one with intermediate retention time. The heteroaggregate is actually decomposed according to Le Châtelier's principle. Components A and B are separated by the column, causing the reaction in Eq. 5d to proceed in reverse.

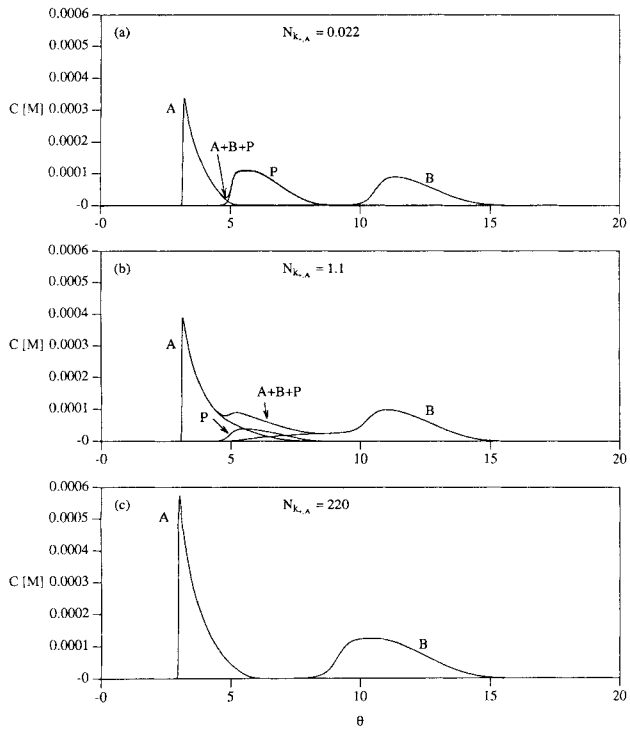

Figure 10. Effect of mixed aggregation on separation for product eluted between reactants.

Note how the mixed aggregate decomposes into the reactants as reaction rate increases.

The peak of B in the bottom chromatogram is shifted to the middle to a small degree because of the time spent in the P form. This principle can be applied to drive any reversible reaction backwards if the product can be eluted between its two reactants. Such a procedure may be incorporated into the design of an effective separation scheme employing heteroaggregation.

The clean resolution of reactants is possible only if the product elutes between the reactants. If the product elutes to either side of the reactants, the product still decomposes, but resolution of the reactants is lost. Since both reactants elute to the same side of the product, they stay together long enough to convert back to product. Homoaggregates do not exhibit this dependency on elution, since there is only one reacting species on either side of the reaction expression. Just as with homoaggregation, retention times of the solutes can also shift as a result of interconversion.

General Applications and Scaling. If the objective is to achieve the maximum concentration of combined solute forms (minimum separation of the individual forms), one should operate at conditions that maximize the values of $Da_{k_{\pm m}}$, $N_{k_{\pm m}}$, and $\Phi^2_{k_{\pm m}}$ while maintaining the low values of N_{f_i} and N_{p_i}. This can be accomplished by increasing the reaction rates (perhaps by increasing the temperature), by decreasing the flow rates, or by increasing the particle size. Decreasing the reaction rates, increasing the flow rate, or decreasing the particle size will have the opposite effect, allowing the various forms to be separated. Concentration and equilibrium distribution can also be increased or decreased to control the effective reaction rates to achieve these goals.

Heteroaggregation has already been used in the area of chiral separations by promotion of complexes with one member of a chiral pair. As shown in the current study, chromatography can be used to reverse the complexation and recover the desired product. The controlling parameter for the recovery of pure solutes is in elution order; the product should elute between the reactants. In general, the control of elution order can be used to drive any type of reaction against thermodynamically favored equilibrium, by separating the desired solute from other solutes; the industrial implications of the idea were reviewed by Langer et al. (1969). Heteroaggregation may also be used to characterize stationary phases through kinetic studies (Chu and Langer, 1985).

The simulations presented have clearly shown that aggregation complicates the dependence of plateau and peak shape on concentration, flow rate, particle size, temperature (can change reaction rates), and pH (can change equilibrium distribution and reaction rates). In scaling up chromatography processes, flow rate, column length, and particle size usually change. The values of most of the dimensionless groups in Table 1 will be altered by such changes. Control of the various mass transfer dimensionless groups for scale-up has been studied previously for nonreacting systems (Lee et al., 1989). However, the $N_{k_{\pm m}}$, $Da_{k_{\pm m}}$, and $\Phi^2_{k_{\pm m}}$ groups must also be considered when reactions are present. Even though required changes for scaling-up, such as flow rate, column length, and particle size, will alter these groups, operating concentration and $k_{\pm m}$ (through changes in temperature) can be varied to keep these key dimensionless groups constant. When the dimensionless groups cannot be kept constant, detailed models, such as VERSE, facilitate exploration of scaling conditions.

Summary and Conclusions

Aggregation, common in biochemical systems, can produce complex effluent histories that depend on many system parameters. The VERSE model was able to closely represent an experimental dimerizing system and a complex multiaggregate system from the literature. A detailed study of a simulated dimerizing system was conducted under all three major operating modes: frontal, elution, and displacement. Dimensionless group analysis was shown to be a good predictor of the plateau shape and peak resolution; the definitions of the groups were also shown to yield insight into how the plateau shape or peak resolution may be controlled. When reaction rates are slow relative to convection and mass transfer rates, effluent histories take on the characteristics of multicomponent systems. Frontal and displacement modes exhibit multiple plateaus, and the elution mode shows peak splitting. At $K_m = 10^4\ M^{-1}$ for a dimerizing system, it was shown that the peaks are generally merged or merging when the reaction rate is tenfold greater than the controlling mass transfer rate.

Changes in several physical parameters can alter the relative ratio of the reaction rate to mass transfer rates, and thus affect the plateau shape and peak resolution in similar ways. For homoaggregation, increasing concentration was shown to increase the effective reaction rate, as defined in the numerator of $N_{k_{+m}}$, $Da_{k_{+m}}$, and $\Phi^2_{k_{+m}}$. A shift in the equilibrium distribution also implies that a forward and/or reverse reaction rate change. Increased reaction rate and decreased flow rate both tend to cause the various aggregate forms of a solute to merge into one peak with an intermediate retention time. Decreasing particle radius reduces mass transfer resistance, resulting in a relatively slower reaction rate, and causing aggregates to appear as multiple plateaus or peaks. The degree of resolution does not depend on relative separation between the two aggregates for homoaggregation. Estimation of isotherm and mass transfer parameters, which often depend on the plateau and peak shape and position, may be in the serious error if aggregation occurs in the system and is overlooked. Changes in the flow rate, particle size, and concentration can alter the apparent equilibrium constants.

Reversible heteroaggregation differs in response to changes in relative reaction rate. For two reactants with different retention characteristics, the heteroaggregate decomposes into the reactants, as predicted by Le Châtelier's principle. Unlike homoaggregation, heteroaggregation exhibits a strong dependence on relative retention times for reactants and products. If the product elutes between the reactants, the reactants may be well resolved upon decomposition of the product. If the product elutes before or after the reactants, the product will still be decomposed; however, resolution of the reactants is significantly reduced. The VERSE model presented in this study was shown to represent well complex reaction sequences found in chromatography, even in the presence of significant mass transfer effects.

To maximize concentration of combined solute forms, one should maximize $N_{k_{\pm m}}$, $Da_{k_{\pm m}}$, and $\Phi^2_{k_{\pm m}}$, and maintain the low values of N_{f_i} and N_{p_i}. Heteroaggregation, combined with chromatography, provides a useful way to separate chiral compounds and drive reactions against the thermodynamic equilibrium through selective reaction and controlled elution order. Scaling is complicated by the additional dimensionless groups arising from the presence of reactions in chromatography. The dimensionless group principles developed in this article represent a methodical framework for scaling and analysis of complex reaction-separation systems.

Acknowledgment

This research was supported by NSF grants BCS-8912150 and CBT-8620221. One of the authors (Kevin E. Van Cott) received partial support through a Purdue Chemical Engineering New Directions Honors Summer Research Assistantship. The IMAC data were kindly supplied by Jon Wong, who was supported by a Rohm and Haas fellowship. C. Y. Lee assisted in analyzing the data in Figure 2. The TSK Chelate 5PW IMAC column was supplied by Supelco. Additional computing resources (a Titan P3) were provided by George Goble of ECN and Stardent Corporation. Sam Addington translated Kihara and Tsuruta's work (1988) from Japanese to English.

Notation

a = Langmuir isotherm parameter
A = molecular species
b = Langmuir isotherm parameter, M^{-1}
B = molecular species
Bi = Biot number, ratio of film mass transfer rate to intraparticle diffusion rate
c = dimensionless concentration
C = concentration, M
C_T = maximum exchanger capacity, M
D = dimer
D^∞ = Brownian diffusivity, $cm^2 \cdot s^{-1}$
$Da_{k_\pm}$ = Damkohler Number; ratio of reaction rate to film mass transfer rate
E_b = axial dispersion coefficient, $cm^2 \cdot s^{-1}$
E_p = intraparticle diffusivity, $cm^2 \cdot s^{-1}$
J = J factor, defined by Eq. 12
k_f = film mass transfer parameter, $cm \cdot s^{-1}$
k_+ = forward reaction rate constant (units depend on reaction)
k_- = reverse reaction rate constant (units depend on reaction)
K = equilibrium constant (units depend on reaction)
Ke = size exclusion factor
L = column length, cm
M = monomer
N_c = number of components
N_f = ratio of film mass transfer rate to convection rate
$N_{k_\pm}$ = ratio of reaction rate to convection rate
N_p = ratio of intraparticle diffusion rate to convection rate
P = molecular specie
Pe = Peclet number
r = particle position, cm
R = particle radius, cm
Re = Reynolds number
Sc = Schmidt number
t = time, s
u_o = interstitial velocity, $cm \cdot s^{-1}$
V = volume, mL
x = dimensionless column position
z = column position, cm

Greek letters

ϵ_b = interparticle void fraction
ϵ_p = intraparticle porosity
μ = viscosity, $g \cdot s^{-1} \cdot cm^{-1}$
ξ = particle position
ρ = density, $g \cdot mL^{-1}$
τ = percolation time, s
υ = generation term by reaction or adsorption/desorption
$\Phi^2_{k_\pm}$ = Thiele modulus; ratio of reaction rate to diffusion rate
θ = dimensionless time

Subscripts

b = bulk phase
D = dimer
e = maximum inlet concentration
f = inlet concentration
i, j = component counters
ℓ = adsorption/desorption
m,n = reaction counters
M = monomer
Mo = monomer only
p = particle phase
P = pulse

Superscripts

$\bar{}$ = solid phase

Literature Cited

Anspach, F. B., A. Johnston, H.-J. Wirth, K. K. Unger, M. T. W. Hearn, "High-Performance Liquid Chromatography of Amino Acids, Peptides, and Proteins: XCV. Thermodynamic and Kinetic Investigations on Rigid and Soft Affinity Gels with Varying Particle and Pore Sizes: Comparison of Thermodynamic Parameters and the Adsorption Behavior of Proteins Evaluated from Batch and Frontal Analysis Experiments," *J. Chromatogr.*, **499**, 103 (1990).

Baudin-Chich, V., M. Marden, and H. Wajcman, "Investigation of the Tetramer-Dimer Equilibrium in Haemoglobin Solutions by High-Performance Size-Exclusion Chromatography on a Diol-Column," *J. Chromatogr.*, **437**, 193 (1988).

Blanco, R., A. Arai, N. Grinberg, D. M. Yarmush, and B. L. Karger, "Role of Association on Protein Adsorption Isotherms: β-Lactoglobulin A Adsorbed on a Weakly Hydrophobic Surface," *J. Chromatogr.*, **482**, 1 (1989).

Blundell, T., G. Dodson, D. Hodgkin, and D. Mercola, "Insulin: The Structure in the Crystal and Its Reflection in Chemistry and Biology," *Adv. in Protein Chemistry*, **26**, 279 (1972).

Bruzzesi, M. R., E. Chiancone, and E. Antonini, "Association-Dissociation Properties of Lysozyme," *Biochemistry*, **4**(9), 1796 (1965).

Cann, J. R., "Theory of Electrophoresis of Hybridizing Enzymes with Kinetic Control: Implications for Population Genetics of Electrophoretic Markers," *J. Theor. Biol.*, **127**, 461 (1987).

Chakrabarti, A., and R. Toral, "Computer Simulation of the Aggregation Process in Self-Associating Polymer and Surfactant Systems," *J. Chem. Phys.*, **91**(9), 5687 (1989).

Chothia, C., A. M. Lesk, G. G. Dodson, and D. C. Hodgkin, "Transmission of Conformational Change in Insulin," *Nature*, **302**, 500 (1983).

Chu, A. H. T., and S. H. Langer, "Characterization of a Chemically Bonded Stationary Phase with Kinetics in a Liquid Chromatographic Reactor," *Anal. Chem.*, **57**, 2197 (1985).

Chung, S. F., and C. Y. Wen, "Longitudinal Dispersion of Liquid Flowing Through Fixed and Fluidized Beds," *AIChE J.*, **14**(6), 857 (1968).

Coffman, F. D., and M. F. Dunn, "Insulin-Metal Ion Interactions: The Binding of Divalent Cations to Insulin Hexamers and Tetramers and the Assembly of Insulin Hexamers," *Biochemistry*, **27**, 6179 (1988).

Cramer, S. M., and Cs. Horváth, "Displacement Chromatography in Peptide Purification," *Prep. Chromatogr.*, **1**(1), 29 (1988).

Davankov, V. A., "Separation of Enantiomeric Compounds Using Chiral HPLC Systems. A Brief Review of General Principles, Advances and Development Trends," *Chromatographia*, **27**(9/10), 475 (1989).

Endo, S., and A. Wada, "Theoretical and Experimental Studies on Zone-Interference Chromatography," *Biophys. Chem.*, **18**, 291 (1983).

Fausnaugh-Pollitt, J., G. Thevenon, L. Janis, and F. E. Regnier, "Chromatographic Resolution of Lysozyme Variants," *J. Chromatogr.*, **443**, 221 (1988).

Garcia-Rubio, L. H., "Characterization of Proteins During Aggregation Using Turbidimetry," *Chem. Eng. Comm.*, **80**, 193 (1989).

Golden, F. M., K. I. Shiloh, G. Klein, and T. Vermeulen, "Theory of Ion-Complexing Effects in Ion-Exchange Column Performance," *J. Phys. Chem.*, **78**(9), 926 (1974).

Goto, M., J. M. Smith, and B. J. McCoy, "Parabolic Profile Approximation (Linear Driving-Force Model) for Chemical Reactions," *Chem. Eng. Sci.*, **45**(2) 443 (1990).

Grinberg, N., R. Blanco, D. M. Yarmush, and B. L. Karger, "Protein Aggregation in High-Performance Liquid Chromatography: Hydrophobic Interaction Chromatography of β-Lactoglobulin A," *Anal. Chem.*, **61**, 514 (1989).

Gross, D., A. Skvorak, G. Hendrick, G. Weir, L. Villa-Komaroff, and P. Halban, "Oxidation of Rat Insulin II, but not I, Leads to Anomalous Elution Profiles Upon HPLC Analysis of Insulin-Related Peptides," *FEBS Letters*, **241**(1,2), 205 (1988).

Helfferich, F. G., "Ion Exchange Kinetics—Evolution of a Theory," p. 157, L. Liberti and F. G. Helfferich, eds., *Mass Transfer and Kinetics of Ion Exchange*, (NATO ASI Series E: Applied Sciences, No. 71), Martinus Nijhoff, The Hague (1983).

Hsu, J. T., and U. P. Ernst, "Theoretical Studies of Reaction Chromatograms by the Fast Fourier Transform Technique," *Chem. Eng. Sci.*, **45**(4), 1017 (1990).

Huber, J. F. K., and R. G. Gerritse, "Evaluation of Dynamic Gas Chromatographic Methods for the Determination of Adsorption and Solution Isotherms," *J. Chromatogr.*, **58**, 137 (1971).

Hwang, Y.-L., F. G. Helfferich, and R.-J. Leu, "Multicomponent Equilibrium Theory for Ion-Exchange Columns Involving Reactions," *AIChE J.*, **34**(10), 1615 (1988).

Imoto, T., L. N. Johnson, A. C. T. North, D. C. Phillips, and J. A. Rupley, "Vertebrate Lysozymes," Ch. 21, *The Enzymes*, **VII**, P. D. Boyer, ed., Academic Press, New York (1972).

Jacobson, J., J. Frenz, and Cs. Horváth, "Measurement of Adsorption Isotherms by Liquid Chromatography," *J. Chromatogr.*, **316**, 53 (1984).

Jeffrey, P. D., B. K. Milthorpe, and L. W. Nichol, "Polymerization Pattern of Insulin at pH. 7.0," *Biochemistry*, **15**(21), 4660 (1976).

Karger, B. L., J. N. LePage, and N. Tanaka, "Secondary Chemical Equilibria in High-Performance Liquid Chromatography," *High Performance Liquid Chromatography*, **1**, 113, Academic Press, New York (1980).

Karger, B. L., and R. Blanco, "The Effect of On-Column Structural Changes of Proteins on Their HPLC Behavior," *Talanta*, **36**(1/2), 243 (1989).

Keller, R. A., and J. C. Giddings, "Multiple Zones and Spots in Chromatography," *J. Chromatogr.*, **3**, 205 (1960).

Kihara, H., and H. Tsuruta, "Kinetic Study on Dissociation-Association and Conformational Changes of Proteins by Stopped Flow X-Ray Scattering," *Seikagaku*, **60**(12), 1371 (1988).

Kirkby, N. F., N. K. H. Slater, K. H. Weisenberger, F. Addo-Yobo, and D. Doulia, "An HPLC Technique for Parameter Estimation for Reversed-Phase Chromatography: A Case Study on Cephalosporin C," *Chem. Eng. Sci.*, **41**, 2005 (1986).

Klein, G., "Ion Exchange and Chemical Reaction in Fixed Beds," *Percolation Processes—Theory and Applications*, A. E. Rodrigues and D. Tondeur, eds., Sijthoff & Noordhoff, Alphen aan den Rijn, The Netherlands, 363 (1981).

Klinkenberg, A., "Chromatography of Substances Undergoing Slow Reversible Chemical Reactions," *Chem. Eng. Sci.*, **15**, 255 (1961).

Kroeff, E. P., R. A. Owens, E. L. Campbell, R. D. Johnson, and H. I. Marks, "Production Scale Purification of Biosynthetic Human Insulin by Reversed-Phase High-Performance Liquid Chromatography," *J. Chromatogr.*, **461**, 45 (1989).

Krull, I. S., "The Liquid-Chromatographic Resolution of Enantiomers," *Adv. Chromatogr.*, **16**, 175 (1978).

Kunitani, M. G., R. L. Cunico, and S. J. Staats, "Reversible Subunit Dissociation of Tumor Necrosis Factor During Hydrophobic Interaction Chromatography," *J. Chromatogr.*, **433**, 205 (1988).

Langer, S. H., J. Y. Yurchak, and J. E. Patton, "The Gas Chromatographic Column as a Chemical Reactor," *Ind. Eng. Chem.*, **61**, 10 (1969).

Lee, C. K., Q. Yu, S. U. Kim, and N.-H. Linda Wang, "Mass Transfer Effects in Isocratic Non-Linear Elution Chromatography," *J. Chromatogr.*, **484**, 29 (1989).

Lindner, W., J. N. LePage, G. Davies, D. E. Seitz, and B. L. Karger, "Reversed-Phase Separation of Optical Isomers of Dns-Amino Acids and Peptides Using Chiral Metal Chelate Additives," *J. Chromatogr.*, **185**, 323 (1979).

Loureiro, J., C. Costa, and A. Rodrigues, "Propagation of Concentration Waves in Fixed-bed Adsorptive Reactors," *Chem. Eng. J.*, **27**, 135 (1983).
McKenzie, G. H., W. H. Sawyer, and L. W. Nichol, "The Molecular Weight and Stability of Concanavalin A," *Biochim. Biophys. Acta.*, **263**, 283 (1972).
Mackie, J. S., and P. Meares, "The Diffusion of Electrolytes in a Cation-Exchange Resin Membrane," *Proc. Roy. Soc. London, Ser. A*, **232**, 498 (1955).
McLeod, A. N., A. Auf Der Mauer, and S. P. Wood, "High-Performance Liquid Chromatography of Insulin: Accessibility and Flexibility," *J. Chromatogr.*, **502**, 325 (1990).
Menger, F. M., "On the Structure of Micelles," *Acc. Chem. Res.*, **12**(4), 111 (1979).
Mhatre, R., I. S. Krull, and H. H. Stuting, "Determination of Biopolymer (Protein) Molecular Weights by Gradient Elution, Reversed-Phase High-Performance Liquid Chromatography with Low-Angle Laser Light Scattering Detection," *J. Chromatogr.*, **502**, 21 (1990).
Muramatsu, N., and A. P. Minton, "Hidden Self-Association of Proteins," *J. Mol. Recognit.*, **1**(4), 166 (1989).
Olson, M. O. J., and I. E. Liener, "The Association and Dissociation of Concanavalin A, the Phytohemagglutinin of the Jack Bean," *Biochemistry*, **6**(12), 3801 (1967).
Pettersson, C., A. Karlsson, and C. Gioeli, "Influence of Enantiomeric Purity of a Chiral Selector on Seteroselectivity," *J. Chromatogr.*, **407**, 217 (1987).
Petzold, L. R., "A Description of DASSL: a Differential/Algebraic Equation System Solver," STR, SAND82-637, Livermore, CA (1982).
Sophianopoulos, A. J., and K. E. Van Holde, "Physical Studies of Muramidase (Lysozyme)," *J. Biol. Chem.*, **239**(8), 2516 (1964).
Stevens, F., "Analysis of Protein-Protein Interaction by Simulation of Small-Zone Size-Exclusion Chromatography: Application to an Antibody-Antigen Association," *Biochemistry*, **25**, 981 (1986).
Stevens, F., "Analysis of Protein-Protein Interaction by Simulation of Small-Zone Size-Exclusion Chromatography: Stochastic Formulation of Kinetic Rate Contributions to Observed High-Performance Liquid Chromatography Elution Characteristics," *Biophysical J.*, **55**, 1155 (1989).
Stuting, H. H., I. S. Krull, R. Mhatre, S. C. Krzysko, and H. G. Barth, "High Performance Liquid Chromatography of Biopolymers," *LC-GC*, **7**(5), 402 (1989).
Tyn, M. T., and T. W. Gusek, "Prediction of Diffusion Coefficients of Proteins," *Biotechnol. Bioeng.*, **35**, 327 (1990).
Villermaux, J., "The Chromatographic Reactor," *Percolation Processes—Theory and Applications*, A. E. Rodrigues and D. Tonduer, eds., Sijthoff & Noordhoff, Alphen aan den Rijn, The Netherlands, 539 (1981).
Weinstein, S., M. H. Engel, and P. E. Hare, "The Enantiomeric Analysis of a Mixture of All Common Protein Amino Acids by High-Performance Liquid Chromatography Using a New Chiral Mobile Phase," *Anal. Biochem.*, **121**, 370 (1982).
Whitley, R. D., R. Wachter, F. Liu, and N.-H. L Wang, "Ion-Exchange Equilibria of Lysozyme, Myoglobin, and Bovine Serum Albumin: Effective Valence and Exchanger Capacity," *J. Chromatogr.*, **465** 137 (1989a).
Whitley, R. D., J. M. Brown, N. P. Karajgikar, and N.-H. L. Wang, "Determination of Ion Exchange Equilibrium Parameters of Amino Acid and Protein Systems by an Impulse Response Technique," *J. Chromatogr.*, **483**, 263 (1989b).
Whitley, R. D., "Dynamics of Nonlinear Multicomponent Chromatography—Interplay of Mass Transfer, Intrinsic Sorption Kinetics, and Reaction," PhD Thesis, Purdue University, West Lafayette, IN (1990).
Wilson, E. J., and C. J. Geankoplis, "Liquid Mass Transfer at Very Low Reynolds Numbers in Packed Beds," *Ind. Eng. Chem. Fundam.*, **5**(1), 9 (1966).
Wong, J. W., "Immobilized Metal Affinity Chromatography," MS Thesis, Purdue University, West Lafayette, IN (1990).
Yu, Q., and N.-H. L. Wang, "Computer Simulations of the Dynamics of Multicomponent Ion Exchange and Adsorption in Fixed Beds—Gradient-Directed Moving Finite Element Method," *Computers Chem. Eng.*, **13**(8), 915 (1989).
Zimmerman, J., "Kinetically Controlled Association-Dissociation Reactions on Gel Chromatography," *Biochemistry*, **13**, 384 (1974).

Manuscript received June 28, 1990, and revision Jan. 15, 1991.